INSTALLATION OF NORMAL-CONDUCTING RF ACCELERATING CAVITIES INTO THE SuperKEKB POSITRON DAMPING RING

Tetsuo Abe*, Yasunao Takeuchi, Hiroshi Sakai, Tatsuya Kageyama, Kazuo Yoshino,
Mika Masuzawa, and Takashi Kawamoto,
High Energy Accelerator Research Organization (KEK), Tsukuba, Japan

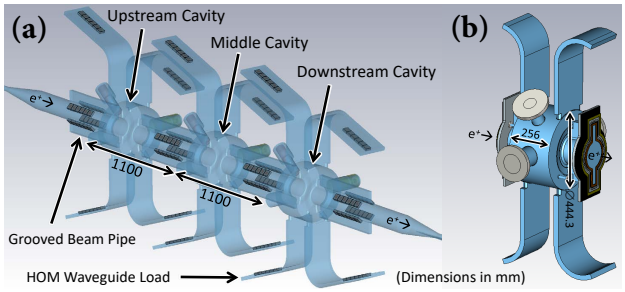

Figure 1: Conceptual diagrams of the accelerating structure for the SuperKEKB positron damping ring. The blue region is a vacuum during operation. (a) Perspective view. The gray region indicates tile-shaped HOM absorbers made of SiC ceramics. (b) Main body of the DR cavity (single cell).

Abstract

We developed an accelerating structure with unique space-saving features for the SuperKEKB positron damping ring. In November, 2016, we installed this characteristic structure into the damping-ring tunnel. In this paper, we present our method and results on this installation.

INTRODUCTION

A positron damping ring (DR) has been constructed to fulfill the requirement for low-emittance positron-beam injection into the main ring (MR) of SuperKEKB [1], where the optics of the SuperKEKB/MRs is based on the nano-beam scheme. For the DR, we proposed the normal-conducting 508.9 MHz accelerating structure shown in Fig. 1a [2], and developed the single-cell standing-wave cavity shown in Fig. 1b (DR cavity), based on the complete higher-order-mode (HOM) damped structure of the normal-conducting RF accelerating cavity system ARES [3] used for (Super)KEKB/MRs.

The accelerating voltage per cavity (cavity voltage (V_c)) in the ARES is 0.5 MV in the specification. Previously, the required total accelerating voltage in the initial DR design was 0.26 MV, meaning that one cavity was enough for DR operation. However, it was shown theoretically that single-bunch instabilities caused by coherent synchrotron radiation would significantly affect the operation if such a total accelerating voltage was used. Now, a total voltage of 1.4 MV is required [4], but the large theoretical uncertainty is still a concern. It should be noted that 1.4 MV is required per the DR design specification, and the hardware (cavity) performance should exceed this requirement. To supply an accelerating voltage higher than 1.4 MV to the DR in the limited space of a sole RF section, which was originally designed for one cavity, we proposed and developed an accelerating structure that can accommodate up to three cavities, as shown in Fig. 1a, where we chose the cavity voltage specification to be 0.8 MV, higher than that of the ARES, guaranteeing a supply of 2.4 MV with three cavities.

To install three cavities at a maximum in the limited space (3.8 m in the beam direction), this accelerating structure has the following space-saving features that are not included in the ARES cavity system:

- The HOM absorbers are all compact tile-shaped silicon carbide (SiC) ceramics;
- The neighboring cavities share a grooved beam pipe [5] in-between;
- The cavity is connected directly to grooved beam pipes without bellows; and
- The grooved beam pipes absorb not only TE modes but also higher-order TM modes, so that we need no additional HOM absorber (e.g., SiC duct) between cavities.

In this accelerating structure, all of the related HOMs, including those moving between the cavities, are damped so that the electromagnetic field in each cavity has high independence. Furthermore, the number of cavities used in this structure is variable, yet it can still be considered a single mechanical structure with solid connections between the components (cavities and beam pipes). This "*multi single cell*" design is the most significant characteristic of this structure. More details are described in Chap. 13 of [1].

We fabricated two production versions of the DR cavity: the first (DR cavity No. 1) in 2012 and the second (DR cavity No. 2) in 2013. DR cavities No. 1 and No. 2 have the same mechanical structure, and tested up to V_c = 0.95 MV at a test stand [6, 7].

In this paper, we report our method and the results of the installation of this characteristic structure into the DR tunnel, performed in November, 2016, with the two-cavity configuration, where a dummy pipe was used in place of the middle cavity, as shown in Fig. 2.

BEAM-PORT FLANGES

Figure 3a and 3c show beam-port flanges, whose perpendicularity to the beam axis is 0.05 mm prescribed in the specifications as a challenge. One flange fits to the other with an allowance of $\approx \pm 0.3$ mm, which is large enough to compensate offsets of the flanges with respect to the DR cavity.

* tetsuo.abe@kek.jp

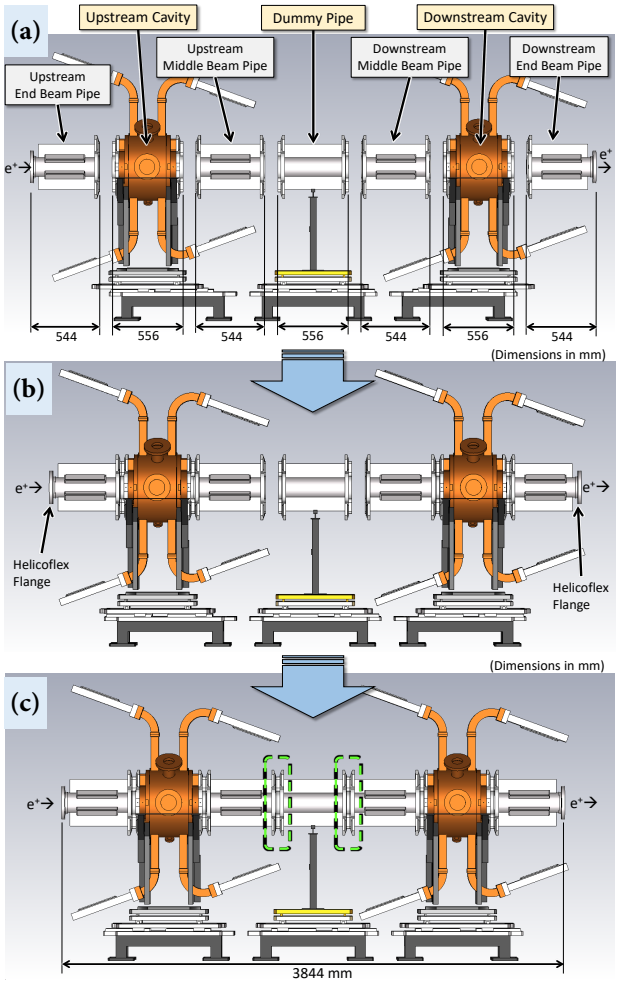

Figure 2: Solid model of the accelerating structure with a two-cavity configuration, showing (a) seven components to be aligned and solidly connected, (b) DR cavities with grooved beam pipes connected, and (c) a single mechanical structure after coalescence.

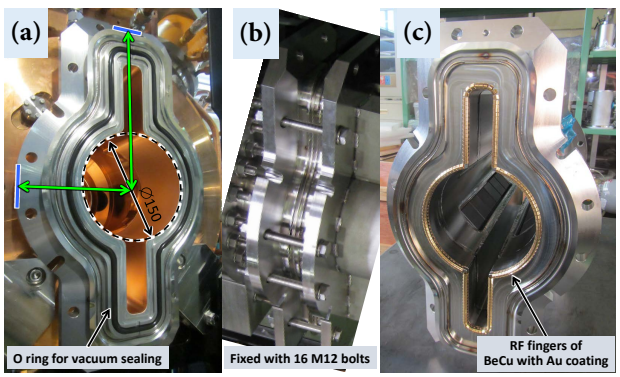

Figure 3: Beam-port flanges of (a) DR cavity and (c) grooved beam pipe, and (b) connection between them.

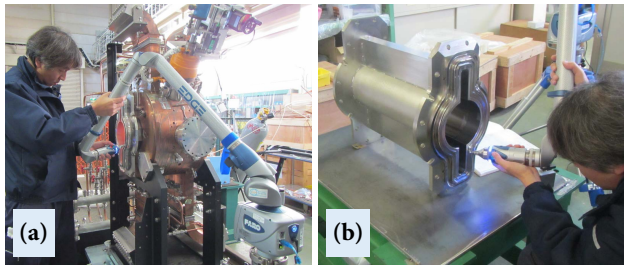

Figure 4: Operator measuring the positions of the beam-port flanges by using FaroArm Edge of (a) DR cavity No. 1 and (b) a dummy pipe.

ALIGNMENT TARGET ACCURACY

The alignment target accuracy is 0.3 mm in the transverse direction with respect to the beam axis[1], taking into account the tolerance of the bellows ducts (200 mm long) in the transverse direction (±1 mm), where only one bellows duct is used in the connection between the accelerating structure and the neighboring vacuum pipe both upstream and downstream.

POSITION MEASUREMENT FOR BEAM-PORT FLANGES

Although each component was machined with 0.05 mm accuracy, some beam-port flanges might be attached with a large tilt angle and/or offset. If the tilt angles and/or offsets are accumulated with the same sign along the accelerating structure, the total might exceed the tolerance at the end. On the other hand, if both positive angles/offsets and corresponding negative ones are present, the total angle and offset can be made small by cancellation. The purpose of our flange measurement is to know the angles and offsets before the installation into the DR tunnel to find the best permutation (direction and order) of the seven components in order to make the accelerating structure as straight as possible.

We used a transportable five-axis coordinate measuring machine (FaroArm Edge), which had a measurement range of 1.8 m in diameter and the precision of repeated measurements at the same position of 0.024 mm in the specifications. Figure 4 shows photos of the actual field of the measurement.

First, we defined the $X - Y$ plane by fitting ≈20 measured points on the flange plane of the upstream beam-port, where the Y axis was defined to aim in the vertically upward direction. Second, we defined a circle by fitting ≈20 measured points on the inner surface of the beam pipe near the upstream beam port, and then defined the origin of the Cartesian coordinate system (O) as a projected point of the fitted-circle center onto the fitted $X - Y$ plane. The Z axis was defined to aim in the positron-beam direction, i.e., upstream to downstream. Third, we defined the $X' - Y'$ plane by fitting ≈20 measured points on the flange plane of the downstream beam-port, where the Y' axis was defined to

[1] This is the same accuracy required for the ARES cavities in the MRs.

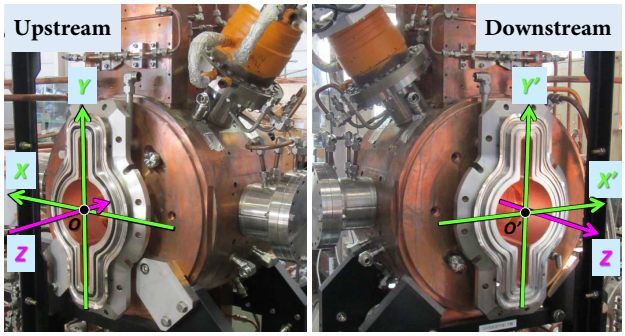

Figure 5: Measurement coordinate systems.

aim in the vertically upward direction. Fourth, we defined a circle by fitting ≈20 measured points on the inner surface of the beam pipe near the downstream beam port, and then defined the origin of the $X'-Y'$ plane (O') as the projected point of the fitted-circle center onto the fitted X'-Y' plane. Figure 5 shows the definitions of the coordinate systems. It should be noted that the beam pipes have geometrical symmetries, and so we defined upstream / downstream and upward / downward as was appropriate.

We defined $(\Delta X, \Delta Y, Z')$ as the coordinate of point O' in the (X, Y, Z) coordinate system, and $(n'_X, n'_Y, \sqrt{1-(n'_X)^2-(n'_Y)^2})$ as the unit vector in the (X, Y, Z) coordinate system normal to the $X'-Y'$ plane. Here, n'_X (n'_Y) is approximately equal to the rotational angle of the $X'-Y'$ plane around the Y (X) axis. Table 1 shows the results of the flange measurement. The sum of all the Z' measurements corresponds to the actual length of the accelerating structure after coalescence of the seven components. The sum is 3842.505 mm, which is ≈ 1.5 mm shorter than the design (3844 mm). However, this difference is much shorter than the tolerance of a bellows duct in the longitudinal direction (±10 mm). The measured offsets are ≈ 0.3 mm or smaller for both ΔX and ΔY as expected from the machining accuracy. However, n'_Y for DR cavity No. 2 (-1.050×10^{-3}) is considerably larger than the others and larger than those expected from the machining accuracy ($\approx 0.3 \times 10^{-3}$ or smaller). In addition, n'_X for DR cavity No. 1 (0.566×10^{-3}) is also large.

For the DR cavities, we also measured the distance between the top plane of the beam-port flange (the blue line shown in Fig. 3a) and the fitted-circle center of the beam pipe, that is, the distance shown in Fig. 3a with a green arrow. The same measurements were taken for the side plane of each beam-port flange of the DR cavities. Table 2 shows the results of this measurement, which will be used for accurate measurement of the cavity misalignment by using a laser tracker after installation.

BEST PERMUTATION

The beam pipes have the following rotational symmetries: 180-degree rotation with respect to the beam axis, and 180-degree rotation with respect to the vertical axis (except for the end beam pipes). Consequently, 2048 permutations are possible in the assembly of the seven components. From the measurement results described in the previous section, we can find the best permutation to make the accelerating structure as straight as possible in the DR tunnel. We determined the permutation of the components in the assembly as follows. Because DR cavities have no such symmetry, we first took the sum of n'_X and n'_Y over DR cavities No. 1 and No. 2 (n'_X(cav) and n'_Y(cav), respectively):

$$n'_X(\text{cav}) = 0.766 \times 10^{-3} \text{ and} \quad (1)$$
$$n'_Y(\text{cav}) = -1.214 \times 10^{-3}\,. \quad (2)$$

If the sign of n'_X or n'_Y of the other components is the same as Eq. (1) or (2), the sign is inverted by using the rotational symmetries, as shown in Tab. 3. By defining DR cavity No. 1 to be the Downstream cavity, and the tilt angles and offsets to be compensated as locally as possible, the best permutation is uniquely determined. As the result, the total n'_X and n'_Y values over all the components (n'_X(tot) and n'_Y(tot), respectively) are reduced to the following:

$$n'_X(\text{tot}) = 0.229 \times 10^{-3} \text{ and} \quad (3)$$
$$n'_Y(\text{tot}) = -0.325 \times 10^{-3}\,. \quad (4)$$

In addition, as shown in Fig. 6, the predicted deviation from the beam axis is also significantly improved as compared with the unselected cases.

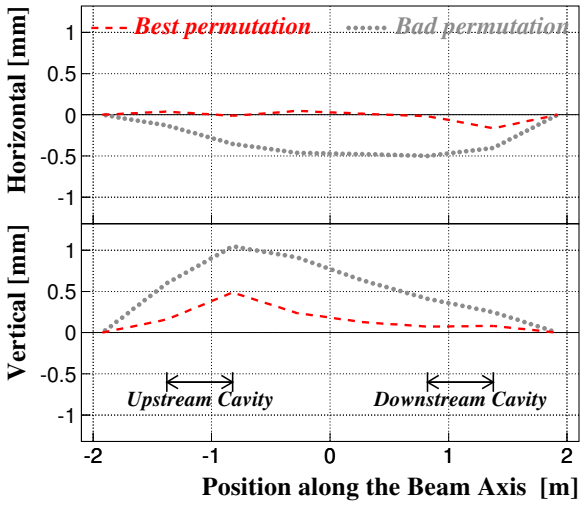

Figure 6: Deviation of the central axis of each component from the beam axis, as predicted by the flange measurement, with the constraint that centers of the most upstream and downstream flanges are on the beam axis. The red dashed lines indicate the best permutation, and the gray dotted lines indicate one of the other permutations (worst case).

DEFINITION OF THE BEAM AXIS DURING THE INSTALLATION

We defined the beam axis by the contact planes of four quadrants of the quadrupole magnets next to the RF sec-

Table 1: Measurement results of the relative positions of the beam-port flanges. The mean values of three independent measurements are shown in mm units. Upper and lower errors correspond to maximum and minimum values among the three measurements, respectively.

	DR cavity No. 1	DR cavity No. 2	Dummy pipe	Middle beam pipe No. 1	Middle beam pipe No. 2	End beam pipe No. 1	End beam pipe No. 2
Z'	$555.991^{+0.003}_{-0.004}$	$555.329^{+0.008}_{-0.010}$	$556.044^{+0.006}_{-0.011}$	$544.077^{+0.006}_{-0.006}$	$543.115^{+0.002}_{-0.002}$	$543.776^{+0.006}_{-0.008}$	$544.173^{+0.001}_{-0.002}$
ΔX	$0.354^{+0.016}_{-0.013}$	$0.009^{+0.007}_{-0.004}$	$-0.073^{+0.010}_{-0.010}$	$0.169^{+0.007}_{-0.014}$	$0.059^{+0.018}_{-0.013}$	$0.117^{+0.014}_{-0.017}$	$0.151^{+0.017}_{-0.023}$
ΔY	$-0.077^{+0.023}_{-0.017}$	$-0.133^{+0.006}_{-0.003}$	$0.054^{+0.010}_{-0.009}$	$-0.001^{+0.014}_{-0.011}$	$-0.053^{+0.003}_{-0.004}$	$0.040^{+0.007}_{-0.006}$	$0.325^{+0.005}_{-0.009}$
$n'_X/10^{-3}$	$0.566^{+0.020}_{-0.037}$	$0.200^{+0.015}_{-0.025}$	$-0.009^{+0.021}_{-0.034}$	$0.172^{+0.001}_{-0.001}$	$0.211^{+0.045}_{-0.026}$	$0.002^{+0.017}_{-0.030}$	$0.161^{+0.045}_{-0.046}$
$n'_Y/10^{-3}$	$-0.164^{+0.011}_{-0.009}$	$-1.050^{+0.014}_{-0.013}$	$0.099^{+0.034}_{-0.025}$	$-0.262^{+0.018}_{-0.017}$	$0.114^{+0.019}_{-0.014}$	$-0.118^{+0.003}_{-0.006}$	$0.296^{+0.024}_{-0.028}$

Table 2: Measured distance between the top or side plane of the beam-port flange of each DR cavity, as shown in Fig. 3a with a green arrow. The mean values of three independent measurements are shown in mm units. Upper and lower errors correspond to the maximum and minimum values among the three measurements, respectively.

	Design	DR cavity No. 1		DR cavity No. 2	
		Upstream	Downstream	Upstream	Downstream
Top	245 ± 0.1	$244.980^{+0.007}_{-0.006}$	$244.987^{+0.034}_{-0.024}$	$244.926^{+0.013}_{-0.023}$	$245.036^{+0.010}_{-0.008}$
Side	150 ± 0.1	$149.996^{+0.002}_{-0.003}$	$149.915^{+0.028}_{-0.020}$	$149.955^{+0.003}_{-0.002}$	$149.975^{+0.007}_{-0.006}$

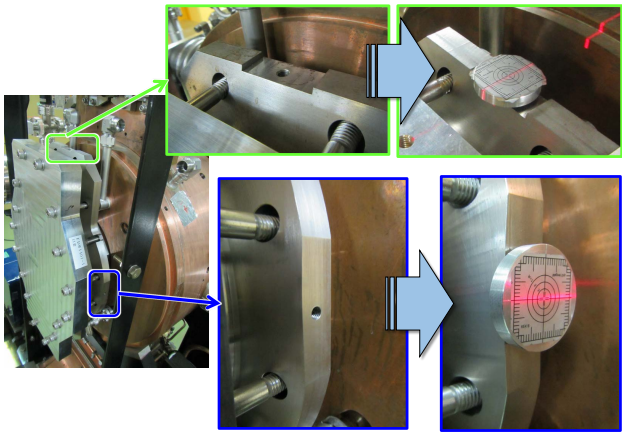

Figure 7: Alignment target attached on each beam-port flange of the DR cavities. The red lines in the right photographs are laser lights from the laser markers.

tion upstream and downstream, where we used laser markers (Tajima ML10N-KJC) and an auto level (Sokkia B40). The line of intersection between two such contact planes is expected to be on the mechanical center of the quadrupole magnet with an accuracy of 0.1 mm or better. We marked the positions of the beam axis on the floor, wall, and ceiling.

ALIGNMENT OF EACH CAVITY

After locating the DR cavities at appropriate positions, we performed alignment of each cavity by using a complete alignment mechanism of each cavity support; we aligned the beam-port flanges by attaching alignment targets on the top and side planes of each flange, as shown in Fig. 7. We performed iterations until all the measured misalignments became 0.3 mm or smaller.

After the above alignment, we connected the grooved beam pipes to the DR cavities, as shown in Fig. 2b, followed by re-alignment of each cavity including the grooved beam pipes. Again, we performed iterations until all the measured misalignments at the targets on both the DR cavities and at the flanges of the beam pipes became 0.3 mm or smaller.

COALESCENCE

We connected DR cavities No. 1 and No. 2 through the dummy pipe, resulting to the single mechanical structure shown in Fig. 2c. Because the straightness could not be perfect at the connections of the flanges of the dummy pipe, we measured the distances between the face-to-face flanges, as shown by the green dashed boxes in Fig. 2c. We found that the nonuniformity of such distances was within the contact range of the RF fingers (Fig. 3c): ±0.9 mm.

MEASUREMENT OF MISALIGNMENT

After the installation, we measured the misalignment of the DR cavities by using the laser tracker (Faro Laser Tracker ION), where we attached target holders on the top and side planes of each beam-port flange of the DR cavities, as shown in Fig. 8, instead of the alignment targets. Here, we redefined the beam axis by using a straight line to connect the holes for the laser-tracker target holder in the reference base plates of the quadrupole magnets next to the RF section. We accurately measured the positions of the top and side planes of the beam-port flanges of the DR cavities with respect to the redefined beam axis. Combining this result and the result obtained by using FaroArm Edge (Tab. 2), we can measure the misalignment of the DR cavities, where the misalignment is the distance between the beam pipe center at the beam-port flanges and the redefined beam axis. Figure 9 shows the results of this misalignment measurement. We performed this measurement twice by locating the laser tracker at different positions, because no

Table 3: The best permutation of the components. The red signs were inverted compared with those in Tab. 1. The sign of n'_X for the dummy pipe was inverted by mistake, but not corrected because it is zero within the measurement precision. The sign of n'_X for the end beam pipe No. 2 was inverted because we defined its Helicoflex flange to be downstream in the flange measurement.

	Upstream end beam pipe	Upstream cavity	Upstream middle beam pipe	Dummy pipe	Downstream middle beam pipe	Downstream cavity	Downstream end beam pipe
	End beam pipe No. 2	DR cavity No. 2	Middle beam pipe No. 1	Dummy duct	Middle beam pipe No. 2	DR cavity No. 1	End beam pipe No. 1
$n'_X/10^{-3}$	−0.161	0.200	−0.172	+0.009	−0.211	0.566	−0.002
$n'_Y/10^{-3}$	0.296	−1.050	+0.262	0.099	0.114	−0.164	+0.118

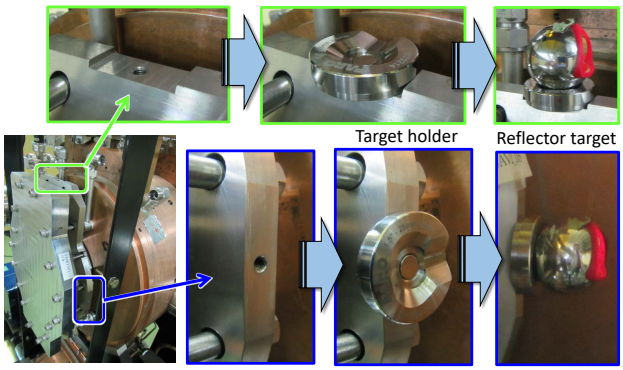

Figure 8: Target holder and 1.5-inch reflector target of the laser tracker. A target holder was attached on each beam-port flange of the DR cavities.

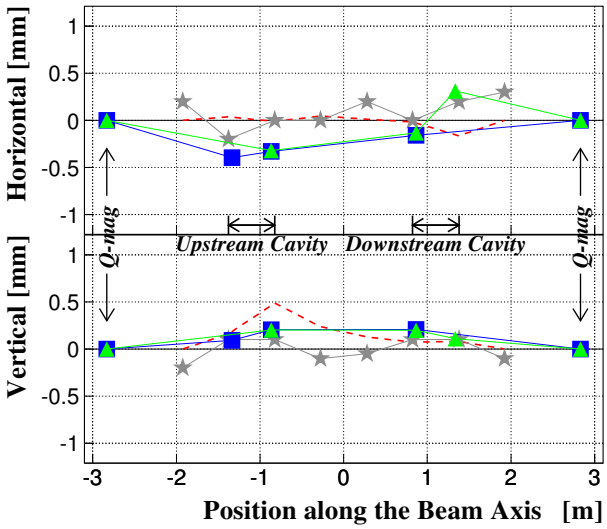

Figure 9: Deviation of the beam-pipe centers from the beam axis. Blue squares (green triangles) are measurements obtained by using the laser tracker located near the Upstream (Downstream) cavity. Predicted deviation for the best permutation (red dashed line from Fig. 6) and measurements using the laser markers and auto level during the installation (gray stars) are also shown for comparison.

position was available where we could see all the beam-port flanges of the DR cavities.

CONCLUSIONS

We have successfully installed a single mechanical structure with unique space-saving features into the DR tunnel. We found the best permutation of components in the assembly by taking flange measurements before the installation, and achieved an alignment accuracy of 0.3 mm as a whole. The accuracy was evaluated by accurate measurements taken before and after the installation.

This new-type of acceleration structure and its installation method can be applied to any longer length of the structure.

ACKNOWLEDGMENTS

The authors are very grateful to the SuperKEKB monitor group for lending their FaroArm Edge to us for this work.

REFERENCES

[1] "SuperKEKB Design Report," 2014; `http://www-superkekb.kek.jp/documents.html`

[2] T. Abe *et al.*, "RF Accelerating Structure for the Positron Damping Ring of the SuperKEKB Injector," in *Proceedings of the 8th Annual Meeting of Particle Accelerator Society of Japan*, 2011. TUPS131 (Japanese).

[3] T. Kageyama *et al.*, "The ARES Cavity for KEKB," *Conf. Proc.*, vol. C9803233, p. 773, 1998.

[4] H. Ikeda *et al.*, "Effect of Coherent Synchrotron Radiation at the SuperKEKB Damping Ring," *Conf. Proc.*, vol. C110904, pp. 3733–3735, 2011.

[5] T. Kageyama, "Grooved beam pipe for damping dipole modes in RF cavities," in *8th Symposium on Accelerator Science and Technology Saitama, Japan*, pp. 116–118, 1991.

[6] T. Abe *et al.*, "High Power Testing of the RF Accelerating Cavity for the Positron Damping Ring at SuperKEKB," in *Proceedings of the 10th Annual Meeting of Particle Accelerator Society of Japan*, 2013. SAP057.

[7] T. Abe *et al.*, "Test Results on RF Accelerating Cavities for the Positron Damping Ring at SuperKEKB," in *Proceedings of the 11th Annual Meeting of Particle Accelerator Society of Japan*, 2014. SAP050.